

Dalton Transactions

Accepted Manuscript



This is an *Accepted Manuscript*, which has been through the Royal Society of Chemistry peer review process and has been accepted for publication.

Accepted Manuscripts are published online shortly after acceptance, before technical editing, formatting and proof reading. Using this free service, authors can make their results available to the community, in citable form, before we publish the edited article. We will replace this *Accepted Manuscript* with the edited and formatted *Advance Article* as soon as it is available.

You can find more information about *Accepted Manuscripts* in the [Information for Authors](#).

Please note that technical editing may introduce minor changes to the text and/or graphics, which may alter content. The journal's standard [Terms & Conditions](#) and the [Ethical guidelines](#) still apply. In no event shall the Royal Society of Chemistry be held responsible for any errors or omissions in this *Accepted Manuscript* or any consequences arising from the use of any information it contains.



Journal Name

ARTICLE

pH value manipulated phase transition, microstructure evolution and tunable upconversion luminescence in Yb³⁺-Er³⁺ codoped LiYF₄/YF₃ nanoparticles

Received 00th January 20xx,
Accepted 00th January 20xx

DOI: 10.1039/x0xx00000x

www.rsc.org/

Song Ye^{*a}, Rongxuan Hu^a, Nan Jiang^b, Huyun Wang^a and Deping Wang^a

The pH value plays an important role in controlling the crystallization process and microstructure of the final products in the synthesis of nanocrystals with solvothermal method. This work reported the effect of the mother solution pH value on the precipitation of LiYF₄ and YF₃ nanoparticles, as well as the microstructure evaluation of YF₃ from bowknot-like to spindle-like shape. Spectroscopy study suggests there is strong correlation between the upconversion emission properties of the Yb³⁺-Er³⁺ couple and the phase and microstructure of the host. The strongest emissions and lowest red-to-green ratio are observed in the bowknot-like YF₃ nanocrystals with the largest open ends. Further spectral investigation indicates that the phase and microstructure dependent upconversion properties are associated with the upconversion efficiency. The present study is of great importance in the design and synthesis of rare earth ions doped nanocrystals with tunable upconversion properties.

Introduction

Upconversion is a luminescent process in which multiple near-infrared photons can be converted to a high-energy photon in the visible range through either the excited state absorption (ESA), energy transfer upconversion (ETU), cooperative upconversion (CU), or photon avalanche (PA) processes.^{1, 2} Recently, rare earth (RE) ions doped fluoride nanoparticles with upconversion properties have evoked great research interests for their potential applications in solar cells, optical communication, infrared detection and especially biological imaging.³⁻⁶ Compared with the conventional organic fluorophores and semiconductor quantum dots, the RE ions doped upconversion nanocrystals have distinctive advantages, such as sharp emission bandwidths, large anti-stokes shift, free of auto-fluorescence background and high photochemical stability.⁷ Moreover, the excitation wavelength for the doped RE ions is around 980 nm, which is within the biological transmission window and thus leads to deep penetration and reduces tissue damage.^{8, 9}

Inorganic fluorides, such as MLnF₄ and LnF₃ (M= alkali metal

ions; Ln=lanthanide ions) have been regarded as excellent host matrixes for upconversion emission due to their lower phonon energies that can minimize the nonradiative transitions and high chemical stabilities.¹⁰ So far, the RE³⁺-Yb³⁺ (RE=Tm, Er, and Pr) activated upconversion luminescence has been widely reported in NaLnF₄ and LnF₃ (Ln= Y, Lu, and Gd) nanocrystals.^{11, 12} Recently, it has been reported that LiYF₄ nanoparticle is also a promising host for efficient upconversion emission. Compared with NaLnF₄, LiYF₄ nanocrystals not only offer comparable emission strength, but also generate additional emission lines.¹³

As microstructure has great influence on the upconversion properties of RE ions, considerable efforts have been made to control the architecture and morphology of the nanoparticles by using either a hard template or soft directing agents to guide the crystal growth.¹⁴ Besides, the simple solution-phase based soft chemical reaction also provides an effective route to fabricate nanoparticles with controlled microstructure under template-free conditions. During the growth of nano/micro inorganic fluorides with hydrothermal or solvothermal methods, not only their intrinsic structures but also the external factors, such as the starting reactants, the reaction temperature and duration, the precursor solution pH values, and the application of organic surfactants greatly influence the crystallization process, the phase evaluation, and the surface morphology of the precipitated nanoparticles.¹⁵ For example, in the synthesis of NaYF₄ by the hydrothermal route, replacing the fluoride source NH₄F with NaF while keeping other reaction conditions unchanged, the uniform

^a School of Materials Science and Engineering, Tongji University, Shanghai 201806 China. Fax: 86-2169584723; Tel: 86-2169584723; E-mail: yesong@tongji.edu.cn

^b Department of Physics, Arizona State University, Tempe, AZ 85287-1504, USA

† Electronic Supplementary Information (ESI) available: More structural characterization, energy levels that involved in the upconversion process and the photographs of the visible upconversion emission. See DOI: 10.1039/x0xx00000x

NaYF₄ became irregular and meanwhile the smooth surface becomes very coarse.¹⁶ In addition, the amount of Inorganic salt also influences morphological evolution. For example, the synthesized GdF₃ changed from a uniform elliptic nanostructure to a submicroplate by adjusting the amount of BaCl₂.¹⁷ It is also reported that the use of ethylenediamine tetraacetic acid (EDTA) can greatly influence the surface morphology and the structure of LiYF₄.^{18, 19}

In this paper, we reported the effect of the mother solution pH value on the precipitation of Yb³⁺-Er³⁺ codoped LiYF₄ and YF₃ nanoparticles, as well as the microstructure evaluation of YF₃, by using a modified solvothermal method. With the same solution composition but gradually reduced pH values, the YF₃ nanoparticles rather than LiYF₄ nanoparticles were precipitated, and the microstructures of YF₃ gradually evolve from a bowknot-like to a spindle-like shape. Meanwhile, the distribution of the nanobelts that constitute the bowknot-like YF₃ can also be controlled by carefully adjusting the mother solution pH value. It is also discovered that there is a strong correlation between the upconversion emission properties of the Yb³⁺-Er³⁺ couple and the microstructure of the host. The maximum upconversion emission can be observed in the bowknot-like YF₃ with the largest open ends microstructure.

Experimental

Materials

All the chemicals used are of analytical grade. The Ln(NO₃)₃·6H₂O (Ln=Y, Yb and Er) were supplied by the A&C Rare Earth Materials Center. The oleic acid, ammonium fluoride, lithium hydroxide, ethanol, nitric acid and cyclohexane were purchased from Sinopharm Chemical Reagent Co. Ltd.

Synthesis of Yb³⁺-Er³⁺ codoped LiYF₄ / YF₃ nanoparticles

Considering the efficient energy transfer before reaching concentration quenching, the doping concentrations of Yb³⁺ and Er³⁺ were set as 10 mol% and 1 mol%, respectively. The Yb³⁺ and Er³⁺ codoped fluoride nanoparticles were prepared by the modified solvothermal method. First, 10mL LiOH aqueous solution (2M) and 30 mL ethanol and 18 mL oleic acid were mixed by vigorous stirring at 35°C for 10 min. Second, 10 mL Ln(NO₃)₃ (2M, Ln=Y, Yb and Er) aqueous solution were added to the mixture to form a microemulsion system. Third, 2mL (2M) NH₄F was injected into the homogeneous solution and was stirred vigorously for 5 min. Without any adjustment, the pH value of the obtained mother solution was 6.20. Several mother solutions with different pH values (pH = 5.20, 4.20, 3.90, 3.60, 3.00 and 2.00) can be obtained by adding appropriate amounts of diluted nitric acid. Finally, these mother solutions were transferred into Teflon-lined autoclaves and heated at 130 °C for 5h. The precipitated nanoparticles were collected by centrifugation, washed using cyclohexane and ethanol for several times, and dried in vacuum at 60 °C for 24 h. The dried powder samples were pressed into disks of 2 nm thick and 5 nm in diameter for the spectral measurements.

Characterization

The X-ray diffraction (XRD) measurement was carried out using a RigakuD/maxrB 12kW X-ray diffractometer with a scan speed of 5 degree/s. The microstructure of the synthesized nanoparticles was characterized using a JEM-2100F transmission electron microscopy (TEM) operating at 200 kV and a Hitachi S4800 scan electron microscopy (SEM). Upconversion emission spectra were acquired using an Edinburgh FLS920 with an external 980 nm laser as excitation source. The Fourier transform infrared (FTIR) spectra were measured by using BRUKER EQUINOX55. All the measurements were carried out at room temperature.

Results and discussion

We found that the pH value plays an important role in controlling the crystallization process and microstructure of the final products in the synthesis of nanoparticles with the solvothermal method. Fig.1 shows the XRD patterns of the synthesized nanoparticles under different pH values. At the pH value of 6.20, the crystallized nanoparticles are mainly tetragonal LiYF₄: Yb³⁺, Er³⁺ along with a very small amount of cubic LiF. It has been reported that the LiF precipitates can be completely eliminated in the final product by adding excess Y ions.²⁰ As the pH value was reduced, the diffraction peaks belonging to orthorhombic YF₃ appeared, and their intensities increased with decreasing pH value, indicating that the lower the pH value the more the YF₃ nanocrystals were precipitated. By contrast, the diffraction peaks of the LiYF₄ nanoparticles decreased with reducing pH value. When the pH value was lower than 3.00, the diffraction peaks belonging to LiYF₄ became invisible and the final precipitates were YF₃ nanoparticles only. Interestingly, the relative intensities of YF₃ diffraction peaks also changed with the pH value, indicating different preferential growth orientation during the crystallization.

In order to understand the effect of pH value on the crystal

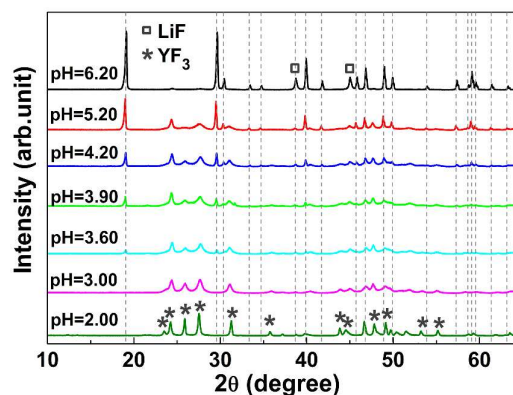


Fig. 1 XRD patterns for the Yb³⁺ and Er³⁺ codoped nanoparticles synthesized with different mother solution pH values. The standard XRD of LiYF₄ (dash lines, JCPDS 81-2254), LiF (open squares, JCPDS 78-1217) and YF₃ (stars, JCPDS 74-0911) are also plotted as references.

precipitation and the morphology evolution, the TEM measurement was carried out for the $\text{Yb}^{3+}\text{-Er}^{3+}$ codoped LiYF_4 and YF_3 nanocrystals synthesized with different mother solution pH values of 6.20, 5.20, 4.20, 3.90, 3.60, 3.00 and 2.00, respectively, as shown in Fig. 2. At the pH value of 6.20, the final products were mainly LiYF_4 octahedrons mixed with a small amount of LiF nanocrystals. This is consistent with the XRD result. When the pH value was reduced to 5.20, both octahedral and bowknot-like nanoparticles can be observed. It has been confirmed by the selected area electron diffraction (SAED) and high-resolution electron microscopy (HREM) that the bowknot-like nanoparticles are YF_3 (see Fig. S1). On a

closer look, the bowknot consists of a bunch of "nano-belts", which are about $1.0 \sim 1.5 \mu\text{m}$ long but only about $20 \sim 40 \text{ nm}$ wide. These nano-belts stick tightly together at the centre knot but stay loose at two ends. With the decrease of the pH value, the ends spread wider, and reach the maximum at the pH value of 3.90. Further reducing the pH value, however, closes the ends. At the pH of value 3.00, some of the YF_3 nanoparticles lose the bowknot-like structure and become spindle-like, as pointed by the arrows in Fig. 2h. At the pH value of 2.00, the ends close completely and all the YF_3 nanoparticles show spindle-like shape.

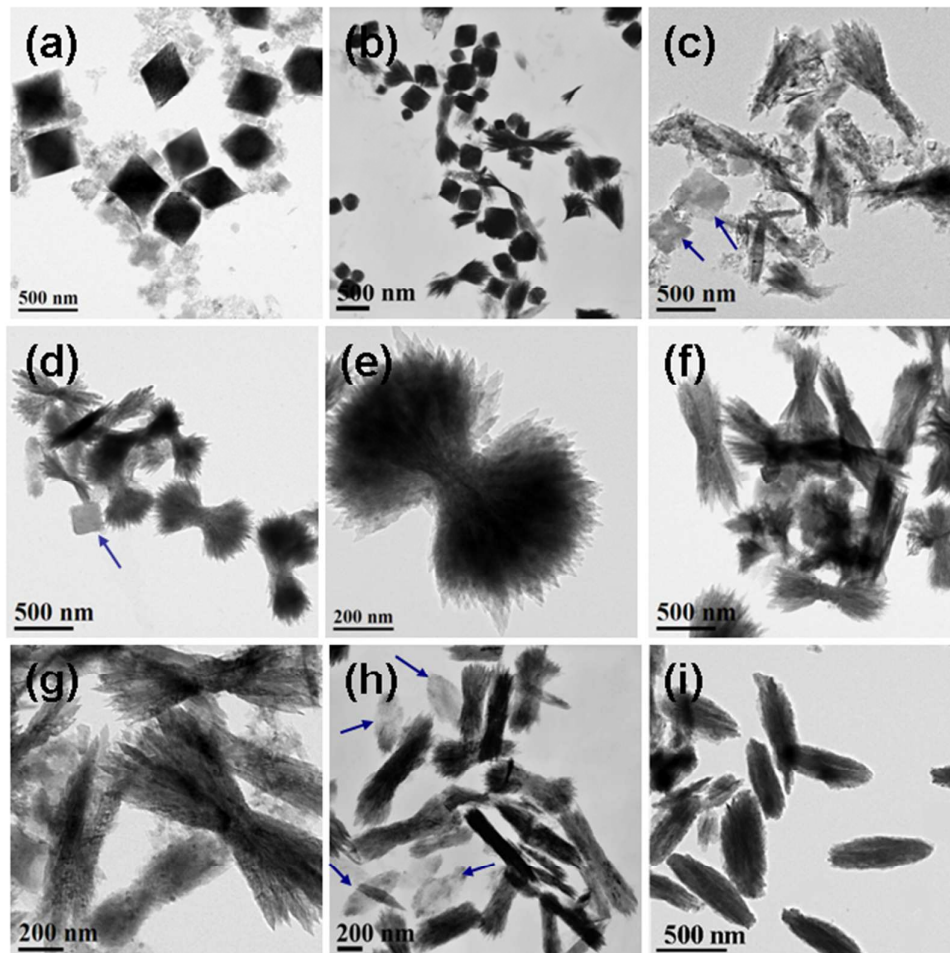


Fig.2 TEM images for the $\text{Yb}^{3+}\text{-Er}^{3+}$ codoped $\text{LiYF}_4/\text{YF}_3$ nanoparticles synthesized with mother solution pH values of 6.20 (a), 5.20 (b) 4.20 (c), 3.90 (d-e), 3.60 (f-g), 3.00 (h) and 2.00 (i), respectively.

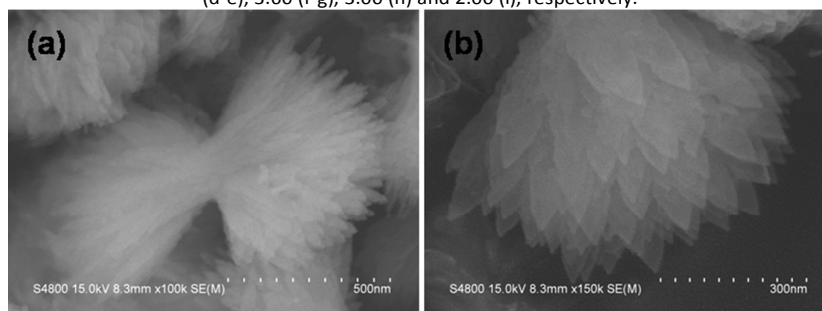


Fig. 3 SEM images for the $\text{YF}_3:\text{Yb}^{3+}, \text{Er}^{3+}$ nanoparticles synthesized with mother solution pH value of 3.90



Journal Name

ARTICLE

The three dimensional morphologies of the bowknot-like YF_3 nanoparticles can be observed in the SEM images in Fig.3, which shows a bowknot with the largest open ends. It is seen that hundreds of YF_3 nanobelts are bundled together to form a bowknot, and each side of the bowknot shows uniformly distributed petal-like substructure. It is roughly estimated that the thickness of the nanobelts that constitute the bowknot-like structure is in the range of several nanometers.

In order to understand the effect of mother solution pH value on the crystallization process of LiYF_4 and YF_3 nanoparticles, as well as the microstructure evolution of YF_3 , the reaction-time-dependent XRD and TEM measurements were carried out for the nanoparticles obtained at the pH values of 6.20, 3.90 and 2.00, in which the pure LiYF_4 nanocrystals, the YF_3 bowknots with the largest open end and the uniform YF_3 spindles were formed, respectively. Fig.4 shows the XRD patterns and the TEM images of the intermediates obtained at different reaction time intervals, from which we can observe that with different mother solution pH values, the intermediates display distinct XRD patterns and morphologies at different reaction periods. At the pH value of 6.20, the initial precipitation was LiF . After 3h of reaction, the peak intensities of LiF decreased, indicating the decrease of LiF concentration. Meanwhile, the peaks of LiYF_4 started to appear. According to the XRD pattern in Fig. 1, after 5h of reaction, almost all the LiF disappeared

and the LiYF_4 dominated. Therefore, we deduce that the growth of LiYF_4 begins with the precipitation of LiF , and then the Y^{3+} and F^- ions may react with LiF to form the LiYF_4 crystal, as schematically shown in Fig 5. This process is similar, however different to the growing of LiYF_4 with hydrothermal method in the presence of ethylenediaminetetraacetic acid (EDTA), in which the YF_3 were firstly precipitated and the LiYF_4 were transformed from YF_3 in the presence of excess Li^+ .²¹ At the pH value of 3.90, the initial precipitation was still LiF . Differently, the YF_3 peaks started to appear after 2h of reaction, and they became much stronger after 3h of reaction. According to the TEM observations (Fig.4 b1-b3), the YF_3 nanobelts were formed after 2h of reaction, and then they self-assembled into the bowknot-like structure with prolonged reaction, as shown in Fig. 5.²² At the pH value of 2.00, no LiF peaks can be observed after 1h of reaction, instead, very broad YF_3 peaks are clearly presented, and those peaks became sharper after 2h and 3h of reaction. Apparently, reducing the mother solution pH value may suppress the precipitation of LiF but enhance the formation of YF_3 nuclei. According to the reaction-time-dependent TEM images (Fig.4 c1-c3), a mass of tiny YF_3 nuclei and small amount of spindle-like YF_3 were formed after 1h of reaction, and then the bigger however loose YF_3 spindles were grown through the aggregation of the nuclei after 3h of reaction. The relative dense YF_3 spindles with

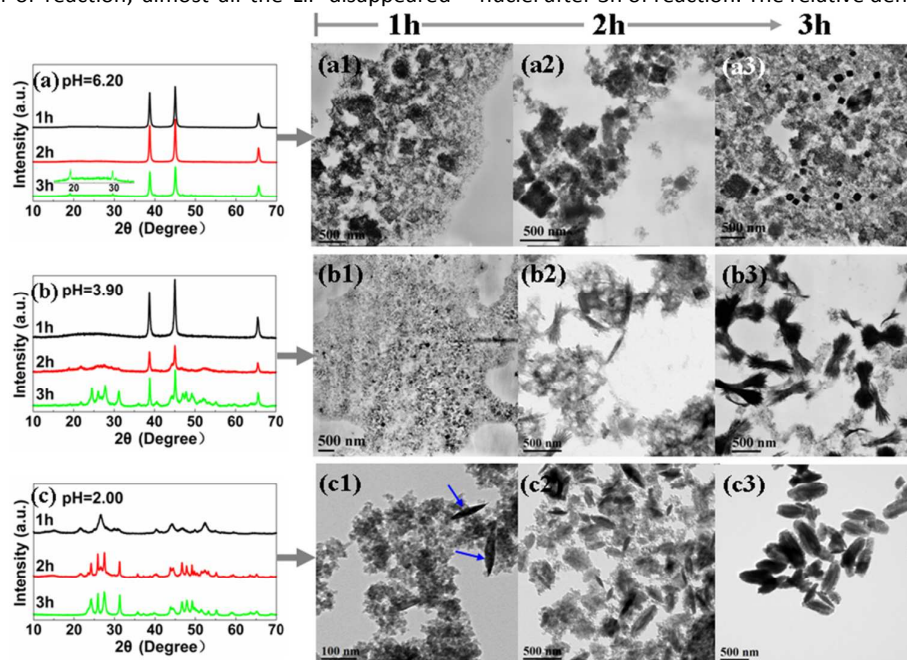


Fig.4 Time dependent XRD patterns and TEM images of the Yb^{3+} - Er^{3+} codoped nanoparticles obtained with different mother solution pH values of 6.20 (a), 3.90 (b) and 2.00 (c), respectively.

Journal Name

ARTICLE

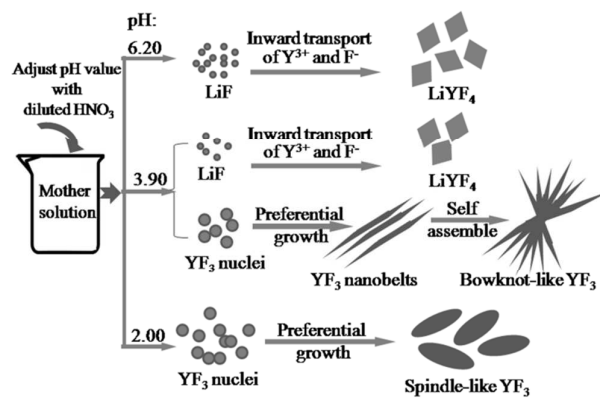


Fig. 5 Schematic illustration for the possible formation processes of LiYF₄ and YF₃ nanoparticles with various morphologies under different mother solution pH values.

an average size of 650 nm long and 220 nm wide were formed after prolonged reaction of 5h (Fig.2 I).

Moreover, it is noticed that the relative diffraction peak intensities of YF₃ precipitations under pH values of 3.90 and 2.00 already shows obvious difference with 3 h reaction, as shown in Fig. 4 (b) and (c). According to the SAED pattern and the FFT image for the intermediates obtained under pH values of 3.90 and 2.00 after 2h reaction (See Fig. S2), the preferential growth orientation of the YF₃ nanobelts is [100], while the preferential growth orientation of YF₃ spindle is [111]. After a prolonged reaction, the nanobelts may self-assemble into the bowknot-like structure while the YF₃ spindle may grow bigger and crystallize better, as shown in Fig.2 (e, i). This indicates that the mother solution pH value greatly influences the morphology of the YF₃ nanocrystals by guiding its preferential growth orientation at the beginning of the reaction.

The preferential formation of orthorhombic YF₃ rather than MYF₄ (M=Li, Na) at lower pH value has also been discussed in the synthesis of fluoride nanoparticles with EDTA as surfactant.²³ In our system, we suggested that the effect of mother solution pH value on the phase transition and microstructure evaluation of LiYF₄/YF₃ nanoparticles can be explained from two points of views: the precipitation of LiF and the deprotonation of the oleic acid. Specifically, high pH value favours the precipitation of LiF due to its lower solubility than in low pH value solution, based on which the LiYF₄ nanoparticles were grown in the presence of excess Y³⁺ and F⁻ ions after prolonged reaction. At reduced pH values, less LiF was precipitated in the mother solution due to the increased solubility, so that less LiYF₄ nanoparticle were formed, until no LiYF₄ peaks can be observed at pH value of 3.00. By contrast, the YF₃ nanobelts were formed under reduced pH value as less Y³⁺ were consumed to form LiYF₄, which were then further

self-assembled as bowknot-like structure with prolonged reaction. The lower the pH value, the more the YF₃ nanobelts can be formed at the beginning of the reaction, so that the YF₃ bowknobs with more open ends can be formed under further reduced pH values (see Fig. S3). On the other hand, after the formation of YF₃, the oleic acid plays an important role in controlling the morphology of the obtained nanoparticles. It is known that the pH value influences the hydrophilic properties of the oleic acid through the deprotonation of the carboxylic group (the higher the pH value, the more hydrophilic the oleic acid will be), which therefore influence the morphology of the oleic.²⁴ As a consequence, the surfactant function of the oleic acid will be alerted after adjusted the mother solution to reduced pH values, which thus influenced the preferential growth orientation of the YF₃ nanoparticles. According to the above experimental results, the spindle-like YF₃ rather than the YF₃ nanobelts were tend to be formed by using the less hydrophilic oleic acid as surfactant. As a result, the concentration of the YF₃ nanobelt decreased, so that the ends of the bowknot-like YF₃ became closer with further reduced pH value to 3.60 and 3.00, and at pH value of 2.00, only the spindle-like YF₃ nanoparticles can be formed, as shown in Fig. 2 (f-i).

Figure 6 shows the upconversion emission spectra of the Yb³⁺-Er³⁺ codoped nanoparticles obtained in different pH solutions, under 980 nm excitation. With the pH value of 6.20, in which the nanoparticles are mainly LiYF₄, the upconversion emission spectrum composes a green emission between 505-570 nm and a red emission between 635-690 nm, corresponding to Er³⁺: (²H_{11/2}, ⁴S_{3/2})→⁴I_{15/2} and Er³⁺: ⁴F_{9/2}→⁴I_{15/2} transitions, respectively (as indicated in Fig. S4).²⁵ Reducing the pH value remarkably increases the overall upconversion emission intensity. The maximum intensity reaches at the pH value of 3.90, in which the YF₃ bowknobs have the largest open ends. While further reducing the pH values to 3.60 and 3.00, when the open ends of YF₃ bowknobs become smaller and some spindle-like YF₃ begin to form, the upconversion emission intensity decreases rapidly. When the pH value was reduced to 2.00, the upconversion emission was almost undetectable in the spindle-like YF₃ nanocrystal for the present measurement setup (small detection slit and low power excitation).

In addition, the intensity ratios of the red to green emission also show pH value dependent, as shown in the inset of Fig.5. It drops rapidly from 2.85 to 0.77 when the pH value reduces from 6.20 to 5.20. Further reducing the pH value, the ratio decreases only slightly and reaches the minimum at the pH value of 3.90. Then it shows slightly increase with further decreasing pH values to 3.60 and 3.00. The photos in Fig.S5

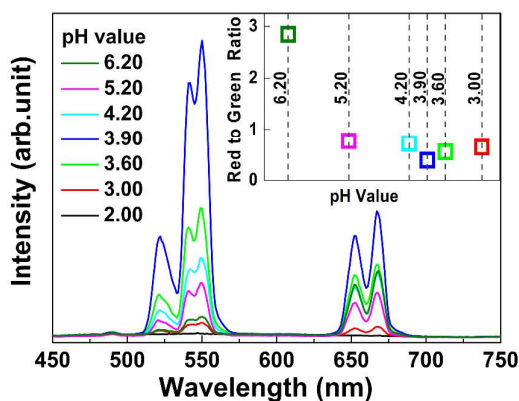


Fig. 6 Upconversion emission spectra of Yb^{3+} - Er^{3+} codoped nanoparticles synthesized with mother solution pH values of 6.20, 5.20, 4.20, 3.90, 3.60, 3.00 and 2.00 respectively. The inset shows the integral intensity ratio of red (635-690 nm) to green (505-570 nm) emissions.

clearly demonstrated the variation of the upconversion emission intensity and the change of the red to green emission ratio.

As discussed above, there is apparently a strong correlation between the upconversion emission properties and the microstructure of the nanoparticles. The strongest emission and lowest red-to-green ratio were observed in the nanocrystals precipitated at the pH value of 3.90, in which the bowknot-like YF_3 nanocrystals have the largest open ends. In order to explain the influence of the host phase and its microstructure on the upconversion emission properties of Yb^{3+} - Er^{3+} couple, the green (${}^2\text{H}_{11/2}$, ${}^4\text{S}_{3/2} \rightarrow {}^4\text{I}_{15/2}$) and the red (${}^4\text{F}_{9/2} \rightarrow {}^4\text{I}_{15/2}$) emissions of Er^{3+} were measured as a function of excitation power in the nanoparticles synthesized with different pH values of 6.20, 4.20, 3.90, and 3.60, respectively, as shown in Fig. 7. According to the upconversion mechanism, the visible emission intensity (I_{em}) is proportional to the excitation power (I_p) through a relationship of $I_{\text{em}} \propto I_p^n$, where n denotes the number of near-infrared photons being absorbed to generate one upconverted photon.²⁶ Fig. 6 shows clearly that under 980 nm excitation, the values of n_G and n_R are consistent with the involvement of two near-infrared photons in generating the green and red emissions. Interesting, it is noticed that both n_G and n_R show similar pH value dependence as the upconversion emission properties shown in Fig. 6, they also have a close relationship with the host structure. In the octahedral LiYF_4 nanoparticles, n_G and n_R equal to 1.50 and 1.80, respectively. With the formation of the bowknot-like YF_3 nanoparticles, these values increase and reach the maximum of 1.83 for the green emission and 1.86 for the red emission when the bowknot-like structure has the largest open ends. And then, n_G and n_R decrease to 1.79 and 1.80 respectively, when the ends of the bowknot became small at a reduced pH value of 3.60. It is reported that inefficient nonradiative channels favour the upconversion process, i.e. higher n value indicates higher upconversion efficiency.^{9, 27} Therefore, these results suggest that the greatly increased upconversion emission intensity is due to the formation of the YF_3 nanoparticles rather than the LiYF_4 , and the upconversion

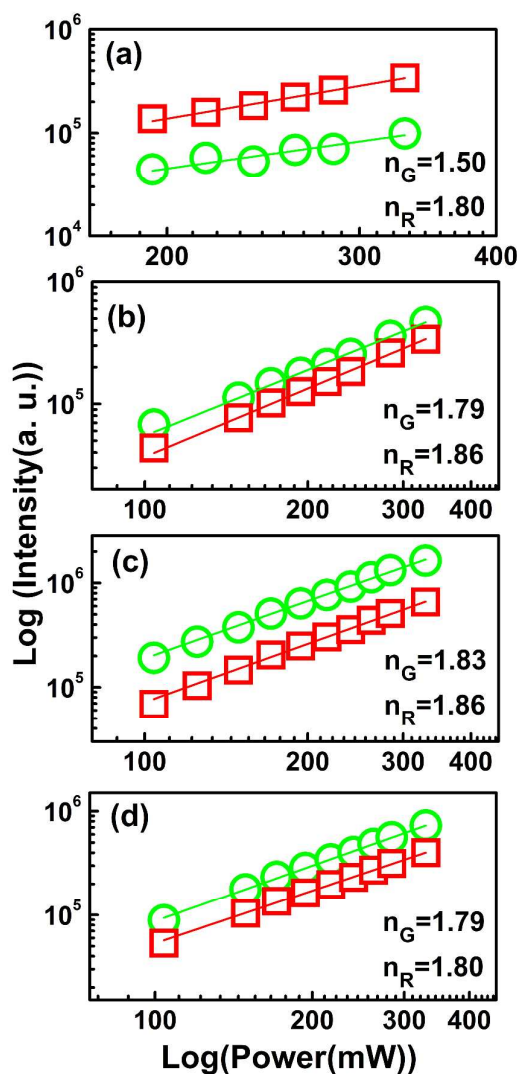


Fig. 7 Excitation power dependence of integrated green (green circle) and red (red square) upconversion emissions for the Yb^{3+} - Er^{3+} codoped nanoparticles synthesized with pH values of 6.20 (a), 4.20 (b), 3.90 (c) and 3.60 (d), respectively. Here, n_G and n_R represent the resulting slopes for the green and the red emissions, respectively.

efficiency is associated with the microstructure of the bowknot-like YF_3 . Specifically, the wider the ends are open, the higher the upconversion efficiency. This YF_3 microstructure dependent upconversion efficiency can be interpreted from the site symmetry point of view. Since a low symmetry favors the upconversion emission,²⁸ the RE ions located on the host surface, at where the site symmetry is lower due to the end of the periodic structure of the crystal, may be responsible for the high upconversion efficiency. In this case, the larger the open ends, the higher the surface-to-volume ratio, the more the RE ions are located on the host surface, and therefore the more efficient upconversion process can be achieved.

In addition, by comparing the variations of n_G and n_R in Fig. 6 we know that with the formation of YF_3 , the upconversion efficiency is greatly increased for the green emission while it is only slightly increased for the red emission. Therefore, an

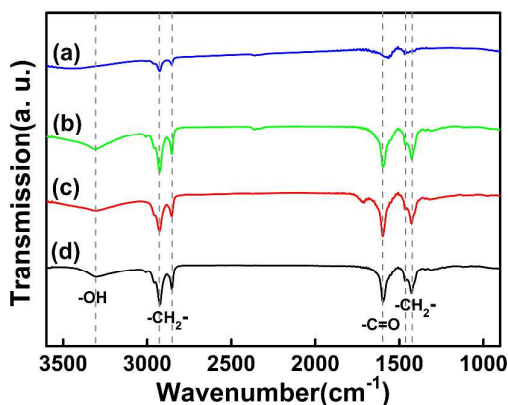


Fig. 8 FTIR spectra of the LiYF_4 and YF_3 nanoparticles synthesized with different mother solution pH values of 6.20 (a), 4.20 (b), 3.90 (c) and 3.60 (d), respectively.

obviously decreased red to green emission intensity ratio can be observed after the formation of YF_3 . The slightly variation of the red to green emission intensity in the bowknot-like YF_3 synthesised under different pH values may also due to the microstructure dependent upconversion efficiency: the larger the open end, the higher the upconversion efficiency is increased for the green emission compared with the red emission, so that the lower the red to green emission ratio.

On the other hand, the presence of organic ligands on the surface of nanoparticles can also influence the upconversion properties.²⁹ In this case, the FTIR spectra for the $\text{Yb}^{3+}\text{-Er}^{3+}$ codoped nanocrystals synthesized with different mother solution pH values were measured to identify the capping ligands on the nanoparticle surface. As shown in Fig. 8, the oleic acid exhibits a broadband absorption around 3320 cm^{-1} , corresponding to the stretching vibration of -OH group; the absorption bands located at 2928 cm^{-1} and 2853 cm^{-1} correspond to the asymmetrical and symmetrical stretching vibration of $\text{-CH}_2\text{-}$; the peak located at 1604 cm^{-1} can be assigned to the stretching vibration of -C=O ; and the bands around 1460 cm^{-1} and 1432 cm^{-1} are due to the deformation vibration of $\text{-CH}_2\text{-}$.³⁰ These peaks indicate the existence of the capping ligands on the surface of these nanoparticles. The drastic increased absorption intensities in the nanoparticles obtained at lower pH values than 6.20 suggests that the bowknot-like YF_3 nanoparticles bear more organic ligands than the octahedral LiYF_4 , which may due to their higher surface-to-volume ratio. Generally, the overall upconversion emission intensity will decrease due to existence of abundant surface quenching centers and surface organic ligands in the nanoparticles with large surface-to-volume ratio.¹⁸ While according to our results, the upconversion emission intensity can be greatly enhanced in the bowknot-like YF_3 with the largest open ends, which indicates the quenching effect due to the surface defects and organic ligands absorptions can be suppressed by the greatly increased upconversion efficiency.

Conclusions

In conclusion, the $\text{Yb}^{3+}\text{-Er}^{3+}$ codoped $\text{LiYF}_4/\text{YF}_3$ nanoparticles with tunable upconversion luminescence were synthesised

with solvothermal method under different mother solution pH values. The effect of pH value on the precipitation of LiYF_4 and YF_3 nanoparticles, as well as the microstructure evaluation of YF_3 nanoparticles can be explained from two points of views: the precipitation of LiF and the deprotonation of the oleic acid. According to the TEM images, LiYF_4 is a large single particle, while YF_3 has a bowknot-like structure or a spindle-like shape. Spectral investigation suggests that there is a strong correlation between the upconversion emission properties of $\text{Yb}^{3+}\text{-Er}^{3+}$ couple and the microstructure of the doping host, the strongest upconversion emission can be observed in the bowknot-like YF_3 with the largest open ends.

Acknowledgements

This work was financially supported by the National Nature Science Foundation of China (No. 50802083), the Innovation Program of Shanghai Municipal Education Commission (No. 14AA037), the Basic Research Project of Shanghai Science and Technology Commission (No. 12JC1408500), and the Fundamental Research Funds for the Central Universities (No. 2011KJ018). The financial support from Bayer-Tongji Eco-Construction and Materials Academy is also acknowledged.

Notes and references

^a School of Materials Science and Engineering, Tongji University, Shanghai 201806 China. Fax: 86-2169584723; Tel: 86-2169584723; E-mail: yesong@tongji.edu.cn

^b Department of Physics, Arizona State University, Tempe, AZ 85287-1504, USA

- G. K. Liu, and B. Jacquier, Tsinghua University Press, 2005.
- F. Zhang, G. B. Braun, Y. F. Shi, Y. C. Zhang, X. H. Sun, N. O. Reich, D. Y. Zhao, and G. Stucky, *J. Am. Chem. Soc.*, 2010, **132**, 2850.
- D. Vennerberg, Z. Q. Lin, *Sci. Adv. Mater.*, 2011, **3**, 26.
- Zhang, P. Steelant, M. Kumar and M. Scholfield, *J. Am. Chem. Soc.*, 2007, **129**, 4526.
- Rumbles, G. *Nature*, 2001, 409, 572.
- (a) S. Schietinger, L. S. Menezes, B. Lauritzen and O. Benson, *Nano Lett.* 2009, **9**, 2477. (b) G. Tian, Z. J. Gu, L. J. Zhou, W. Y. Yin, X. X. Liu, L. Yan, S. Jin, W. L. Ren, G. M. Xing, S. J. Li, Y. L. Zhao, *Adv. Mater.* 2012, **24**, 1226.
- X. S. Zhai, S. S. Liu, Y. L. Zhang, G. S. Qin, and W. P. Qin, *J. Mater. Chem. C*, 2013, **2** 2037.
- Ramasamy, P. Chandra, S. W. Rhee and J. Kim, *Nanoscale*, 2013, **5** 8711.
- J. W. Zhao, Y. J. Sun, X. G. Kong, L. J. Tian, Y. Wang, L. P. Tu, J. L. Zhao, and H. Zhang, *J. Phys. Chem. B*, 2008, **112**, 15666.
- F. Wang, Y. Han, C. S. Lim, Y. H. Lu, J. Wang, J. Xu, H. Y. Chen, C. Zhang, M. H. Hong and X. G. Liu, *Nature*, 2010, **463**, 1061.
- (a) S. Schietinger, L. S. Menezes, B. Lauritzen and O. Benson, *Nano Lett.* 2009, **9**, 2477. (b) F. Shi, Y. Zhao, *J. Mater. Chem. C*, 2014, **2**, 2198. (c) H. Liu, H. Wang, X. Li, and D. P. Chen, *J. Mater. Chem.*, 2009, **19**, 3546. (d) J. J. Wang, H. W. Song, W. Xue, B. Dong, S. Xue, B. T. Chen, W. Yu, and S. Zhang, *Nanoscale*, 2013, **5**, 3412. (e) S. J. Zen, J. J. Xiao, Q. B. Yang, and J. H. Hao, *J. Mater. Chem. C*, 2012, **22** 9870.
- (a) C. X. Li, J. Yang, P. P. Yang, H. Z. Lian, J. Lin, *Chem. Mater.* 2008, **20**, 4317. (b) R. X. Yan, Y. D. Li, *Adv. Funct. Mater.* 2005, **15**, 763.

13. (a) V. Mahalingam, F. Vetrone, R. Naccache, A. Speghini, and J. A. Capobianco, Naccache, *Adv. Mater.*, 2009, **21**, 4025. (b) G. Y. Chen, T. Y. Ohulchansky, A. Kachynski, H. Agren, and P. N. Prasad, *ACS Nano*, 2011, **5**, 4981. (c) L. M. Zhang, Z. X. Wang, Z. X. Lu, K. Xia, Y. Deng, S. Li, C. X. Zhang, Y. F. Huang, N. Y. He *J. Nanosci. Nanotechnol.*, 2014, **14** 4710. (d) V. Mahalingam, R. Naccache, F. Vetrone, J. A. Capobianco, *Chem. Commun.*, 2011, **47**, 3481. (e) S. S. Liu, X. Y. Guo, X. S. Zhai, D. Zhao, K. Z. Zheng, G. S. Qin, W. P. Qin, *J Nanosci. Nanotechnol.* 2014, **14**, 3718.
14. F. Wang, X. G. Liu, *Chem. Soc. Rev.*, *Chem. Soc. Rev.*, 2009, **38**, 976.
15. (a) G. F. Wang, Q. Peng, Y. D. Li, *Acc. Chem. Res.*, 2011, **44**, 322. (b) F. Zhang, J. Li, J. Shan, L. Xu, D. Y. Zhao, *Chem. Eur. J.* 2009, **15**, 11010.
16. C. X. Li, J. Yang, Z. W. Quan, P. P. Yang, D. Y. Kong, J. Lin, *Chem. Mater.* 2007, **19**, 4933.
17. Q. Zhao, W. Lu, N. Guo, Y. C. Jia, W. Z. LV, B. Q. Shao, M. M. Jiao, H. P. You, *Dalton Trans.* 2013, **42**, 6902.
18. W. Gao, H. R. Zheng, E. J. He. Y. Lu, F. Q. Gao, *J. Lumin.*, 2014, **152**, 44.
19. X. Y. Zhang, M. Q. Wang, J. J. Ding, J. P. Deng, C. X. Ran, Z. Yang, *Dalton Trans.*, 2014, **43**, 5453.
20. Q. Zhang, B. Yan, *Inorg. Chem.*, 2010, **49**, 6834.
21. J. W. Zhao, X. M. Liu, D. Cui, Y. J. Sun, Y. Yu, Y. F. Yang, C. Du, Y. Wang, K. Song, K. Liu, S. Z. Lu, X. G. Kong, H. Zhang, *Eur. Inorg. Chem.*, 2010, 1813.
22. S. H. Huang, X. Zhang, L. Z. Wang, L. Bai, J. Xue, C. X. Li, P. P. Yang, *Dalton Trans.*, 2012, **41**, 5634.
23. (a) X. Y. Zhang, M. Q. Wang, J. J. Ding, *RSC Adv.*, 2014, **4**, 29165. (b) D. L. Gao, W. Gao, P. Shi, L. Li, *RSC Adv.*, 2013, **3**, 14757.
24. (a) T. B. Ren, Q. M. Liu, H. Lu, H. M. Liu, X. Zhang, J. Z. Du, *J. Mater. Chem.*, 2012, **22**, 12329. (b) J. Y. Qin, Q. M. Liu, J. X. Zhang, J. Chen, S. Chen, Y. Zhao, J. Z. Du, *Appl. Mater. Inter.*, 2015, DOI: 10.1021/acsami.5b03222.
25. (a) R. X. Hu, S. Ye, H. Y. Wang, W. J. Zhang, Z. Y. Zhang, J. Lin, D. P. Wang, *J. Nanosci. Nanotechnol.*, 2015, **15**, 368. (b) X. Y. Zhang, M. Q. Wang, J. J. Ding, X. H. Song, J. Liu, J. Y. Shao, Y. J. Li, *RSC Adv.*, 2014, **4**, 40223.
26. (a) S. W. Hao, W. Shao, H. L. Qiu, Y. F. Shang, R. W. Fan, X. Y. Guo, L. L. Zhao, G. Y. Chen, and C. H. Yang, *RSC Adv.*, 2014, **4**, 56302. (b) J. W. Zhao, X. M. Liu, D. Cui, Y. J. Sun, Y. Yu, Y. F. Yang, C. Du, Y. Wang, K. Song, K. Liu, S. Z. Lu, X. G. Kong, H. Zhang, *Eur. Inorg. Chem.* 2010, 1813.
27. Y. J. Sun, Y. Chen, L. J. Tian, Y. Yu, X. G. Kong, J. W. Zhao and H. Zhang, *Nanotechnology*, 2007, **18**, 275609.
28. (a) C. Z. Zhao, X. G. Kong, X. M. Liu, L. P. Tu, F. Wu, Y. L. Zhang, K. Liu, Q. H. Zeng, and H. Zhang, *Nanoscale*, 2013, **5**, 8084. (b) Y. F. Bai, K. Yang, Y. X. Wang, X. R. Zhang, Y. L. Song, *Optics Commun.* 2008, **281**, 2930. (c) P. Ramasamy, P. Chandra, S. W. Rhee, J. Kim, *Nanoscale*, 2013, **5**, 8711.
29. (a) G. De, W. P. Qin, J. S. Zhang, J. S. Zhang, Y. Wang, C. Y. Cao, and Y. Cui, *J. Lumin.* 2006, **119-120**, 258. (b) F. Vetrone, J. C. Boyer, J. A. Capobianco, *J. Appl. Phys.* 2004, **96**, 661
30. (a) X. G. Yu, Y. Shan, G. C. Li, K. Z. Chen, *J. Mater. Chem.* 2011, **21**, 8104. (b) D. Q. Gao, X. Y. Zhang, W. Gao, *J. Appl. Phys.* 2012, **111**, 033505.

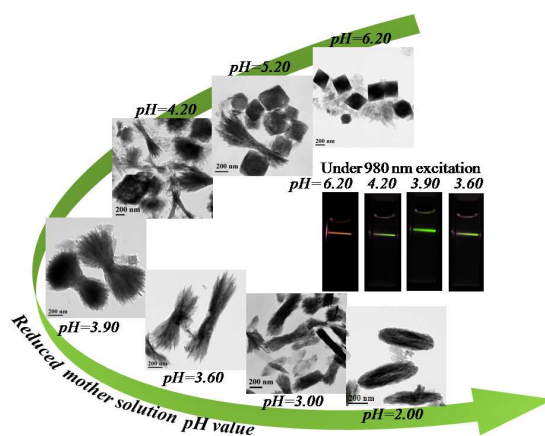
pH value manipulated phase transition, microstructure evolution and tunable upconversion luminescence in Yb^{3+} - Er^{3+} codoped $\text{LiYF}_4/\text{YF}_3$ nanoparticles

Song Ye^{1*}, Rongxuan Hu¹, Nan Jiang², Huiyun Wang¹, and Deping Wang¹

1. School of Materials Science and Engineering, Tongji University, Shanghai 201806 China

2. Department of Physics, Arizona State University, Tempe, AZ 85287-1504, USA

Email: yesong@tongji.edu.cn



Effect of pH value on the phase transition, microstructure evolution and upconversion properties were demonstrated in Yb^{3+} - Er^{3+} codoped $\text{LiYF}_4/\text{YF}_3$ nanoparticles.